



# Aptamer based electrochemiluminescent thrombin assay using carbon dots anchored onto silver-decorated polydopamine nanospheres

Yuanyuan Liu<sup>1</sup> · Yanhua Zhao<sup>1</sup> · Qi Fan<sup>1</sup> · Malik Saddam Khan<sup>1</sup> · Xiaojian Li<sup>1</sup> · Yong Zhang<sup>1</sup> · Hongmin Ma<sup>1</sup> · Qin Wei<sup>1</sup>

Received: 1 December 2017 / Accepted: 11 December 2017 / Published online: 8 January 2018  
© Springer-Verlag GmbH Austria, part of Springer Nature 2017

## Abstract

An electrochemiluminescent (ECL) aptamer based assay is described for thrombin. It is based on the use of carbon dots (C-dots) placed on polydopamine nanospheres loaded with silver nanoparticles (PDANS@Ag) and with probe DNA (pDNA). The PDANS possess high specific surface and can load a large number of C-dots. The AgNPs, in turn, enhance the ECL emission of the C-dots. Platinum functionalized graphene (Gr-Pt) can connect capture DNA (cDNA). The ECL nanoprobe consisting of PDANS@Ag/C-dots was placed on a glassy carbon electrode modified with Gr-Pt/cDNA/BSA via hybridization between cDNA and pDNA. On applying voltages from  $-1.8$  V to 0 V, a strong ECL signal is generated. If thrombin is added, it will bind to cDNA. This leads to the release of pDNA from the electrode surface and a decrease in ECL intensity. Response to thrombin is linear in the  $1.0$  fmol·L<sup>-1</sup> to  $5.0$  nmol·L<sup>-1</sup> concentration range, with a  $0.35$  fmol·L<sup>-1</sup> detection limit. The assay is stable, repeatable and selective, which demonstrates its clinical applicability.

**Keywords** Silver nanoparticles · Platinum functionalized graphene · Nanoprobe · Hybridization chain reaction · Probe DNA · Capture DNA · Biomimetic polymer

## Introduction

Thrombin (TB) is a serine protease in the bloodstream which can convert soluble fibrinogen into insoluble fibrin and promote blood coagulation [1]. It plays significant roles in a variety of life processes and relates to many diseases, such as thromboembolic disease, inflammation reactions, cardiovascular diseases, and anticlotting therapeutics [2]. Therefore, the sensitive determination of TB is of great importance in clinical research and diagnosis. Aptamers are functional oligonucleotides obtained by SELEX. They can bind specific target

molecules such as small organic compounds, metal ions, proteins and metabolites with high selectivity [3, 4]. Aptamers exhibit many advantages including long-term storage stability, ease synthesis, high specificity and affinity [5]. Electrochemiluminescence (ECL) has become too much important analytical technique in clinic, environment, and pharmaceutical owing to its excellent controllability, simple instrumentation and high sensitivity [6]. The combination of the high selectivity of aptamers with the high sensitivity of the ECL technique has led to the emergence of ECL sensor [7].

While some traditional ECL luminescent materials (for example, Ru(bpy)<sub>3</sub><sup>2+</sup> and its derivatives) have been well studied [8, 9], increasing attention has been concentrated on searching new luminescent materials to develop new ECL systems. It has been found that many kinds of semiconductor quantum dots (QDs) behave ECL activity [10]. However, the application of cadmium-containing QDs and lead-containing QDs is generally limited due to their toxicity, poor biocompatibility and stability [11]. Carbon dots (C-dots) have attracted considerable attention because of their unique optical and electronic properties [12]. Carbon dots (C-dots) is a kind of

**Electronic supplementary material** The online version of this article (<https://doi.org/10.1007/s00604-017-2616-2>) contains supplementary material, which is available to authorized users.

✉ Hongmin Ma  
mahongmin2002@126.com

<sup>1</sup> Key Laboratory of Interface Reaction & Sensing Analysis in Universities of Shandong, School of Chemistry and Chemical Engineering, University of Jinan, Jinan 250022, China

environmentally friendly material compared with the metal semiconductor QDs. However, C-dots are difficult to be immobilized on the electrode. The ECL efficiency of pure C-dots is low, which limit its application in ECL assay. On account of the above problems, many efforts have focused on fixing C-dots and enhancing the ECL efficiency of C-dots. For the past few years, some researchers found that loading QDs on appropriate supports can substantially improve the analytical sensitivity of QDs-based ECL methods. These supports include SiO<sub>2</sub> [13], graphene [14], carbon nanotube [15], noble metal nanoparticles [16] and so on. Thus, it is expected that the loading of C-dots on an appropriate support as ECL labels may provide higher sensitivity in TB analysis.

Mussel-inspired polydopamine, a kind of biomimetic polymer, has excellent biocompatibility, biodegradability and excellent affinity to most of the solid surface [17, 18]. Due to this incredible feature, it has been extensively investigated for various applications including drug delivery [19], surface modification [20], metal deposition [21] and others. The remarkable quenching effect of polydopamine nanosphere (PDANS) towards the ECL of the tris-(2,2'-bipyridine)ruthenium (Ru(bpy)<sub>3</sub><sup>2+</sup>) was firstly investigated and was used to develop an ECL immunosensor in our previous work [22]. The quenching mechanism can be explained that the excited states of Ru(bpy)<sub>3</sub><sup>2+</sup> can be annihilated by Quinone units via energy transfer. In addition, PDANS has other excellent properties such as high specific surface area and unique adhesion ability. PDANS possess surface functional groups (-NH<sub>2</sub>), exhibiting an outstanding versatile active nature, which may connect thiolate C-dots via thiol-amine [23]. In the present work, we reported for the first time that the PDANS were used as a carrier to load C-dots based on the large specific surface area, the unique adhesion property. It is well known that Ag NPs can reduce the electron-relay shield between semiconducting ECL emitters and the working electrode due to the outstanding conductivity and the accelerated electron-hole injecting rate [24]. To achieve further signal amplification, Ag NPs was used to decorate the PDANS and improve the ECL response of C-dots.

For the detection of TB, a signal-off type ECL assay was successfully designed. Platinum functionalized graphene (Gr-Pt) was used as a sensing platform to fix capturing DNA (cDNA), while C-dots loaded PDANS@Ag (PDANS@Ag/C-dots) were used as ECL Nano probe to label probing DNA (pDNA). The Gr-Pt increased the surface area of sensing platform and improved the electron transfer rate. The PDANS@Ag/C-dots was introduced into the electrode interface via the hybridization chain reaction between cDNA and pDNA, which generate a strong ECL signal by applying a voltage from -1.8 V to 0 V. The target analyses TB can specifically recognize the cDNA, leading to the release of the signal probe from the electrode surface and the decrease of ECL intensity. The ECL assay exhibited a high sensitivity

based on the multiple signal amplification effects of the composite Nano probe. Significantly, the new method may be quite promising in clinical assays.

## Experimental

### Preparation of Gr-Pt

Graphene oxide (GO) was prepared from graphite powder by a modified Hummers method [25]. 20 mL 4.5 mg·mL<sup>-1</sup> GO dispersion was sonicated for 30 min. And then 3.18 mL 8.5 mg·mL<sup>-1</sup> H<sub>2</sub>PtCl<sub>6</sub>·H<sub>2</sub>O solution was added under stirring. After the pH value of this mixture was adjusted to 10.0 using ammonia, 3 mL 2 mg·mL<sup>-1</sup> NaBH<sub>4</sub> aqueous solutions was slowly added and stirred for 12 h under room temperature. Subsequently, the product was obtained by centrifugal separation and dried by freeze-drying. Finally, the final solid sample was re-dispersed in ultrapure water.

### Preparation of C-dots

C-dots were synthesized through hydrothermal treatment of citric acid according to a previous report [26]. 2 g of citric acid was put into a 100 mL beaker and heated to 200 °C by a heating device for 30 min until the white solid changed to an orange red liquid. Then 10 mg·mL<sup>-1</sup> of NaOH solution was added dropwise into the orange liquid under vigorous stirring until the pH was adjusted to neutral. The C-dots solution was stored at 4 °C before use.

### Preparation of PDANS@Ag

PDANS were synthesized through oxidative polymerization of DA according to the literature with some modifications [27]. Typically, 100 mg of DA was added to the mixture of 100 mL 0.01 mol·L<sup>-1</sup> Tris-buffer NaBH<sub>4</sub> (pH = 8.8) and 50 mL of isopropyl alcohol. And then the mixture was stirred for 24 h under dark. The product was collected by centrifugal separation (9500 rpm, 15 min) and washed three times with ultrapure water to remove unreacted dopamine. It was then dried by freeze-drying. 2 mg PDANS were dispersed in 5 mL H<sub>2</sub>O in a vial by sonication, followed by adding 278 mg of sodium citrate and freshly prepared AgNO<sub>3</sub> solution (20 mL 0.025 mol·L<sup>-1</sup>). The mixture was stirred at room temperature for 3 h under nitrogen atmosphere. Subsequently, the product was centrifuged and washed with ultrapure water for three times. The resultant product of PDANS@Ag was dispersed in water for further use.

### Preparation of PDANS@Ag/C-dots

Firstly, thiolate C-dots was synthesized as follows, 15.4 mg cysteine and 95.8 mg EDC were added into 20 mL prepared C-dots solution, and the mixture was reacting at room temperature for 24 h. The resultant solution was further dialyzed for 2 days in a dialysis bag (retained molecular weight: 3000 Da) to remove byproducts and uncoupled compounds. Then 2 mg PDANS@Ag were put into 1 mL thiolate C-dots solution and vibrated for 6 h. Subsequently, the mixture was centrifuged and washed with ultrapure water for three times to remove unbound C-dots. Finally, the product was dispersed in PB with a final volume of 1.0 mL for further use.

### Preparation of pDNA-PDANS@Ag/C-dots

Briefly, 200  $\mu\text{L}$  2.5  $\mu\text{mol L}^{-1}$  pDNA was added into 1.0 mL 2 mg  $\text{mL}^{-1}$  PDANS@Ag/C-dots solution with stirring for 12 h at 4  $^{\circ}\text{C}$ . The product was purified by centrifugation and washed with ultrapure water three times. The resultant pDNA-PDANS@Ag/C-dots conjugate was stored at 4  $^{\circ}\text{C}$  before use.

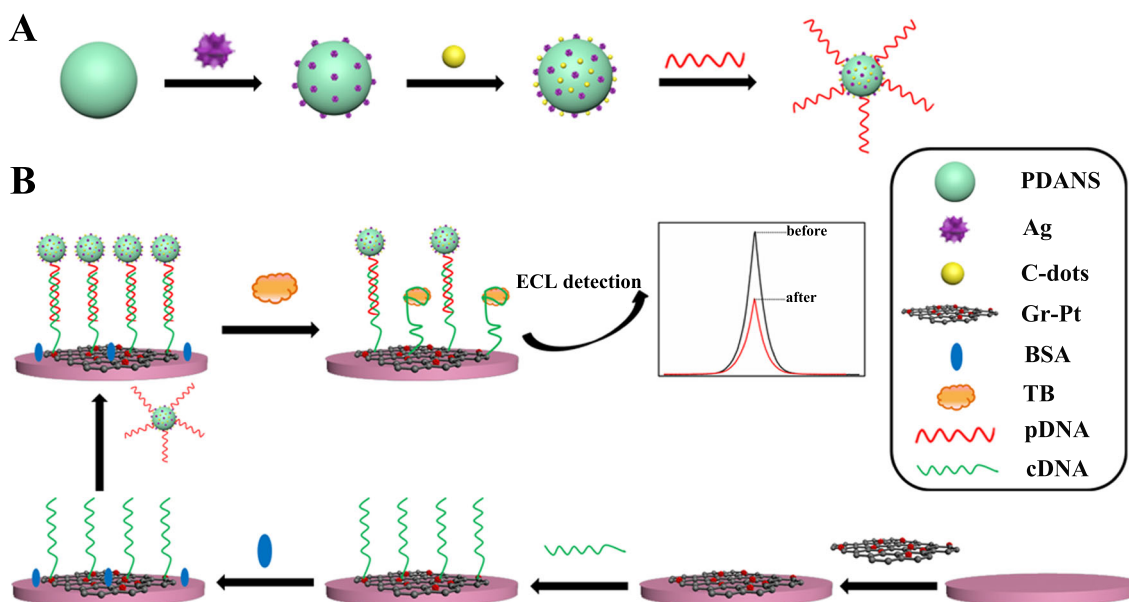
### Fabrication of the working electrode

The process of electrode modification is illustrated in Scheme 1. Prior to modification, glassy carbon electrode (GCE, 4 mm in diameter) was polished sequentially with 0.3 and 0.05  $\mu\text{m}$   $\alpha\text{-Al}_2\text{O}_3$  power, followed by ultrasonic

cleaning with ethanol and rinsing thoroughly with ultrapure water. 6  $\mu\text{L}$  of Gr-Pt solution was added on the pretreated GCE. After being dried under ambient conditions, the modified GCE was immersed in PB (1/15  $\text{mol}\cdot\text{L}^{-1}$ ) containing 1.5  $\mu\text{mol}\cdot\text{L}^{-1}$  cDNA for 12 h at 4  $^{\circ}\text{C}$ . Subsequently, 3  $\mu\text{L}$  1% BSA was dropped onto the GCE to block possible remaining active sites. After washing with PB (pH 7.4), the resultant modified electrode was incubated with 100  $\mu\text{L}$  of pDNA-PDANS@Ag/GQDs conjugate at 37  $^{\circ}\text{C}$  for 2 h. Eventually, the electrode was washed thoroughly with PB to remove un-hybridized pDNA-PDANS@Ag/GQDs conjugate. The finished modified working electrode (GCE/Gr-Pt/cDNA/BSA/pDNA-PDANS@Ag/GQDs) was stored in the 4  $^{\circ}\text{C}$  refrigerator for further use.

### ECL detection

The modified working electrode was incubated in TB standard solution with a series of different concentrations for 40 min at 37  $^{\circ}\text{C}$ , followed by thoroughly washing with the PB (1/15  $\text{mol}\cdot\text{L}^{-1}$ ) to remove unbound TB and replaced pDNA-PDANS@Ag/C-dots conjugate. The modified working electrode was measured in a quartz cell at room temperature in 10 mL PB containing 50  $\text{mmol}\cdot\text{L}^{-1}$  of  $\text{K}_2\text{S}_2\text{O}_8$ . The continuous potential scanning was applied on the working electrode for electrochemical measurements from  $-1.8$  V to 0 V at a scanning rate of 0.1  $\text{V}\cdot\text{s}^{-1}$  and the photomultiplier tube (PMT) was set at 800 V. The ECL signals were recorded by the MPI-F flow-injection chemiluminescent detector.



**Scheme 1** Schematic illustration of pDNA-PDANS@Ag/C-dots preparation (a) and the ECL aptasensor fabrication process (b)

## Results and discussion

### Choice of materials

Graphene exhibits the structure of two-dimensional sheet composed of  $sp^2$ -bonded carbon atoms. It has unique physical properties such as superior electric conductivities, high surface areas (theoretical specific surface area of  $2620 \text{ m}^2/\text{g}$ ), excellent mechanical strength and elasticity. Compared to multi-wall carbon nanotubes and spherical carbon nanoparticles, graphene is a more charming supporting material for biosensor applications. Pt nanoparticles are deposited onto graphene sheets via synchronous reduction of  $\text{H}_2\text{PtCl}_6$  and graphene oxide suspension using  $\text{NaBH}_4$ . Gr-Pt nanocomposite is used to modify the electrode, which increases the surface area to fix a large number of cDNA and improved the electronic transmission rate. In our work, it is found that Gr-Pt modified electrode can enhance ECL performance. Compared with the Gr-Au and Gr-Ag modified electrodes, we find that Gr-Pt modified electrode has achieved the best effect (Fig. S1).

### Characterization of nanomaterials

To testify the successful synthesis of the Gr-Pt nanocomposite, the characterization methods including SEM, TEM, XRD and EDS were employed. Fig. 1a, b show SEM and TEM image of the GO-Pt nanocomposite, a large number of homogeneous nanoparticles are observed on the surface of two-dimensional graphene Nano sheet. XRD pattern of the Gr-Pt verifies the composition profile (Fig. 1c). The  $2\theta$  angular ranged from  $10^\circ$  to  $80^\circ$  were explored at a scan rate of  $10^\circ \text{ min}^{-1}$ . The broad peak located at  $2\theta \approx 24.5^\circ$  is assigned to the graphite [28]. The diffraction peaks at  $40.2^\circ$ ,  $46.5^\circ$ , and  $67.8^\circ$  can be indexed to the (111), (200), and (220) planes of the face-centered cubic phase of Pt [29]. The EDS (Fig. 1d) exhibits that the sample is mainly composed of C, O and Pt elements, indicating that Gr-Pt compound was synthesized successfully.

As shown in Fig. 2a, TEM image suggests that C-dots are monodispersed well and uniform. The diameters of the C-dots are distributed mainly in the range of  $9 \sim 10 \text{ nm}$ . The fluorescent properties of C-dots are shown in Fig. S2-S4. As observed from the SEM image in Fig. 2b, after self-polymerization of dopamine, monodisperse PDANS are

**Fig. 1** SEM (a) and TEM (b) images of Gr-Pt nanocomposite; XRD (c) and EDS (d) of Gr-Pt nanocomposite

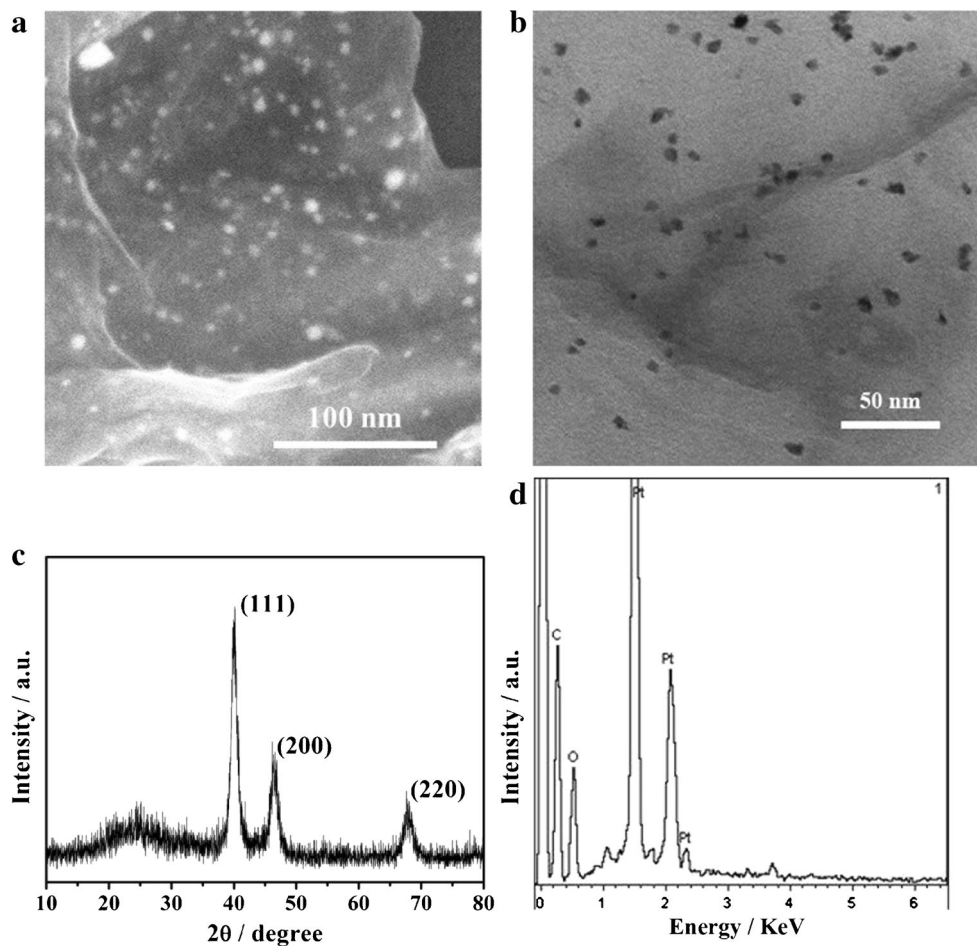
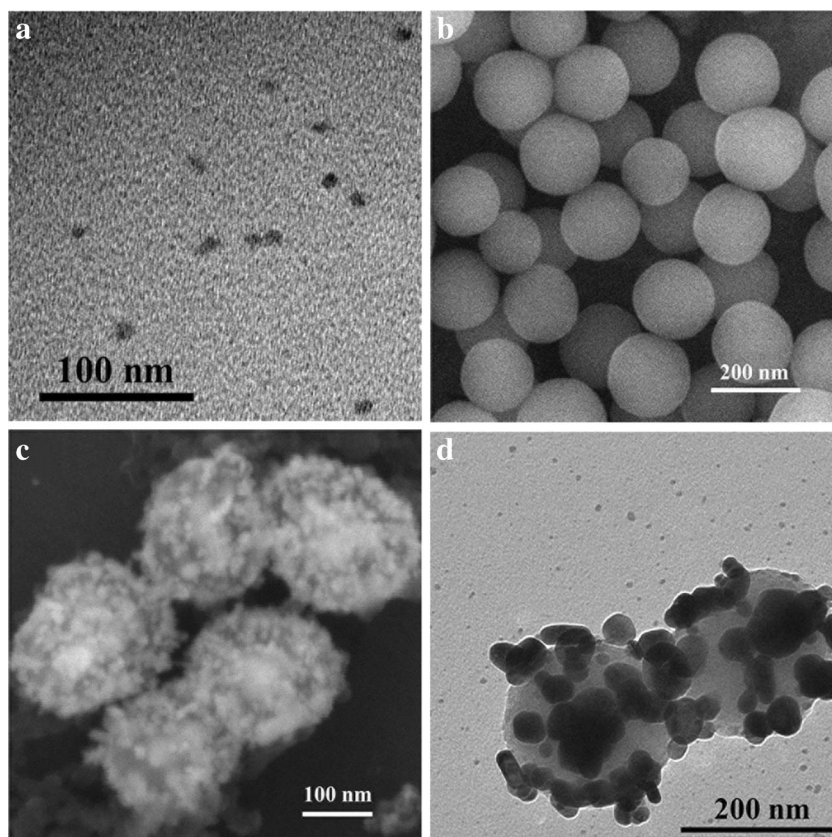


**Fig. 2** TEM (a) image of C-dots; SEM image of PDANS (b); SEM (c) and TEM (d) images of PDANS@Ag



obtained with a diameter of approximately 180 nm. The morphologies of the PDANS@Ag are shown in Fig. 2c, d. It can be seen from the SEM image the Ag NPs are homogeneously adhered to the surface of PDANS, and the globular structure of PDANS is maintained. The TEM image also proves that Ag NPs have grown on the surface of PDANS.

UV-vis spectroscopy analysis provides more effective information on the successful immobilization of C-dots onto the PDANS@Ag. As shown in Fig. S2, the monotonic broad band absorption spectrum for PDANS (curve a) is similar to a previous report [17], which in accordance with the well-known optical characteristics of natural eumelanin related to photo-protection. It can be seen from the inserted photograph that the UV-vis spectrum of PDANS@Ag (curve b) presents the characteristic peak of Ag at about 410 nm. The UV-vis spectrum of C-dots (curve c) shows an obvious absorption peak at about 345 nm. The UV-vis spectrum of PDANS@Ag/C-dots (curve d) presents the characteristic peaks of Ag and C-dots, indicating that PDANS@Ag/C-dots nanocomposite is successfully synthesized.

### Characterization of pDNA-PDANS@Ag/C-dots probe

In order to certify the successful conjugation of pDNA and PDANS@Ag/C-dots, Fig. 3a shows the corresponding ECL-potential profiles of the immobilization process of pDNA-

PDANS@Ag/C-dots probe, which investigated in PB (pH = 7.5) containing  $50 \text{ mmol}\cdot\text{L}^{-1} \text{K}_2\text{S}_2\text{O}_8$ . Negligible ECL peak is obtained at the PDANS@Ag modified electrode (curve a). At the PDANS@Ag/C-dots modified electrode, one strong cathodic ECL can be obtained at  $-1.75 \text{ V}$ , revealing that PDANS@Ag/C-dots can react with  $\text{K}_2\text{S}_2\text{O}_8$  to generate ECL (curve b). By contrast, as pDNA was connected on PDANS@Ag/C-dots, the ECL intensity is weakened significantly (curve c). This phenomenon can be explained that pDNA hindered the electron transfer between  $\text{K}_2\text{S}_2\text{O}_8$  and luminescent reagent. It indicates that the pDNA-PDANS@Ag/C-dots conjugate is successfully fabricated.

### Characterization of ECL assay

Cyclic voltammetry (CV) test was performed to investigate the stepwise fabrication of the working electrode in  $5 \text{ mmol}\cdot\text{L}^{-1} [\text{Fe}(\text{CN})_6]^{3-/4-}$  containing  $0.1 \text{ mol}\cdot\text{L}^{-1} \text{KCl}$  with a scan rate of  $0.1 \text{ V}\cdot\text{s}^{-1}$ . The potential is in the range from  $-0.2$  to  $0.6 \text{ V}$ . As shown in Fig. 3b, the bare GCE exhibits a couple of reversible redox peaks (curve a). After the Gr-Pt is modified on the electrode surface, the peak current increases owing to its excellent conductivity (curve b). Subsequently, the peak current decreases when the electrode is successively modified with cDNA (curve c), BSA (curve d), and pDNA-PDANS@Ag/C-dots (curve e). This is because the formation

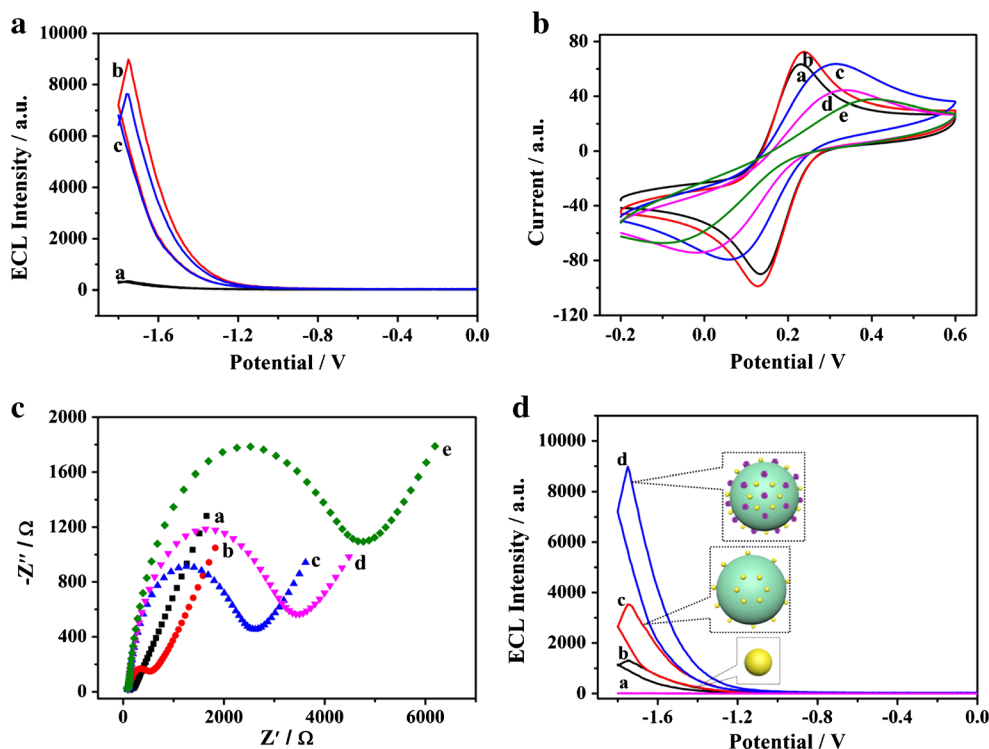


**Fig. 3** The corresponding ECL-potential profiles (a) of the GCE modified with different materials which investigated in PB (pH = 7.5) containing  $50 \text{ mmol}\cdot\text{L}^{-1} \text{K}_2\text{S}_2\text{O}_8$ . ECL-potential curves of GCE/PDANS@Ag (curve a), GCE/PDANS@Ag/C-dots (curve b), GCE/pDNA-PDANS@Ag/C-dots (curve c); CV test which performed in  $5 \text{ mmol}\cdot\text{L}^{-1} [\text{Fe}(\text{CN})_6]^{3-/4-}$  containing  $0.1 \text{ mol}\cdot\text{L}^{-1} \text{KCl}$  with a scan rate of  $0.1 \text{ V}\cdot\text{s}^{-1}$ , the CV curves (b) obtained for different modified electrodes, the bare GCE (curve a), GCE/Gr-Pt (curve b), GCE/Gr-Pt/cDNA (curve

c), GCE/Gr-Pt/cDNA/BSA (curve d), GCE/Gr-Pt/cDNA/BSA/pDNA-PDANS@Ag/C-dots (curve e); EIS curves (c) obtained for different modified electrodes in  $[\text{Fe}(\text{CN})_6]^{3-/4-}$  solution, the bare GCE (curve a), GCE/Gr-Pt (curve b), GCE/Gr-Pt/cDNA (curve c), GCE/Gr-Pt/cDNA/BSA (curve d), GCE/Gr-Pt/cDNA/BSA/pDNA-PDANS@Ag/C-dots (curve e); ECL-potential curves (d) of the GCE modified with different signal probes: GCE (curve a), GCE/C-dots (curve b), GCE/PDANS/C-dots (curve c), GCE/PDANS@Ag/C-dots (curve d)

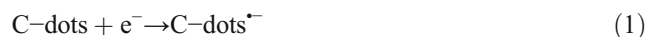
of protein molecule layers with poor conductivity impeded the electron transfer.

In order to further characterize the modified electrode, electrochemical impedance spectrum (EIS) was performed at different modified electrodes to evaluate the interfacial changes of the electrode in the fabricated process. The Nyquist plots of AC impedance spectroscopy were recorded from 0.1 to 105 Hz in a solution containing  $0.1 \text{ mol}\cdot\text{L}^{-1} \text{KCl}$  and  $2.5 \text{ mmol}\cdot\text{L}^{-1} [\text{Fe}(\text{CN})_6]^{3-/4-}$ . It is usually considered that the diameter of the semicircle is the equivalent of the electron transfer resistance ( $R_{ct}$ ), which acts as a significant role in the electron transfer kinetics of the redox probe [30]. As shown in Fig. 3c, the bare GCE displays a small semicircle (curve a).  $R_{ct}$  increases slightly after Gr-Pt is dropped on the electrode (curve b), which is ascribed to the significantly improved electrical conductivity of Gr-Pt, indicating that Gr-Pt can accelerate the electron transfer. Subsequently, a consecutive increase of the  $R_{ct}$  is obtained when the cDNA (curve c), BSA (curve d) and pDNA-PDANS@Ag/C-dots (curve e) are successively incubated on the electrode, demonstrating the formation of protein molecule layers can hinder the electron transfer. Based on these results of CV and EIS, the working electrode is successfully fabricated as expected.

### The comparison of different signal probes

In order to explore the effect of loading C-dots on PDANS and doping of Ag NPs for ECL signal amplification. Under the same experimental conditions, GCEs are decorated by three kinds of different signal probes respectively, including C-dots (curve b), PDANS/C-dots (curve c) and PDANS@Ag/C-dots (curve d). As illustrated in Fig. 3d, the ECL response of PDANS/C-dots increases to a higher value than that of the pure C-dots. The increase in ECL signal might be attributed to the appropriate support. After PDANS@Ag/C-dots is immobilized on GCE, the ECL response is increased obviously, indicating that Ag can improve the ECL intensity of C-dots.

The possible ECL mechanisms may be illustrated as follows. When the electrode scan from  $-1.8 \sim 0 \text{ V}$ , C-dots immobilized on the electrode are reduced to C-dots $^{\cdot-}$  by charge injection (eq. 1). Simultaneously,  $\text{S}_2\text{O}_8^{2-}$  is reduced to form the strongly oxidative  $\text{SO}_4^{\cdot-}$  radicals (eq. 2). The C-dots $^{\cdot-}$  can further react with  $\text{SO}_4^{\cdot-}$  to produce the excited state of C-dots\* (eq. 3). Then the excited-state of C-dots\* decay to produce emission (eq. 4)



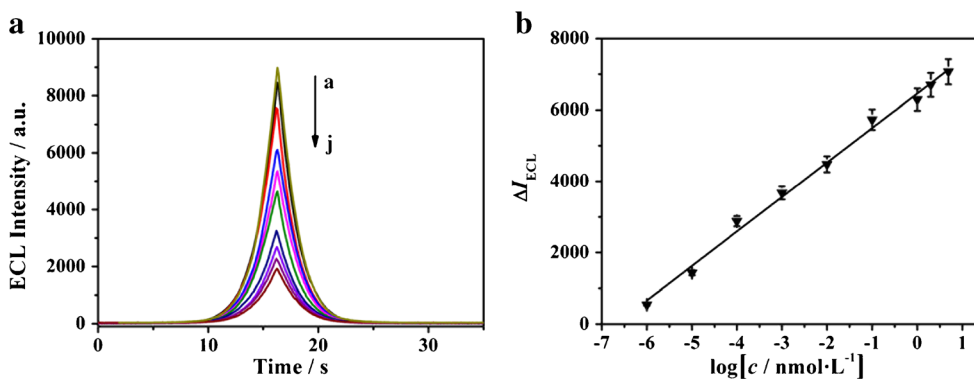
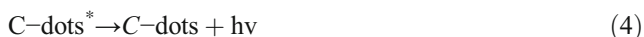
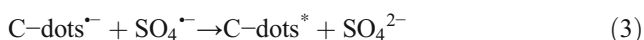
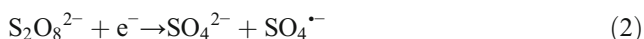


**Fig. 4** ECL response (a) of the modified working electrode to different concentrations of TB: 0 (a),  $1.0 \times 10^{-6}$  nmol·L<sup>-1</sup> (b),  $1.0 \times 10^{-5}$  nmol·L<sup>-1</sup> (c),  $1.0 \times 10^{-4}$  nmol·L<sup>-1</sup> (d),  $1.0 \times 10^{-3}$  nmol·L<sup>-1</sup> (e),  $1.0 \times 10^{-2}$  nmol·L<sup>-1</sup> (f), 0.1 nmol·L<sup>-1</sup> (g), 1.0 nmol·L<sup>-1</sup> (h), 2.0 nmol·L<sup>-1</sup> (i), 5.0 nmol·L<sup>-1</sup> (j) under a voltage from -1.8 V to 0 V (the PMT was set at 800 V); The calibration plot (b) of the ECL assay with different concentrations of TB; Stability of ECL emissions under continuous scanning for 13 cycles in PB

(pH 7.5) containing 50 mmol·L<sup>-1</sup> K<sub>2</sub>S<sub>2</sub>O<sub>8</sub> for detection of 0.1 nmol·L<sup>-1</sup> TB (B); The reproducibility of the aptasensor (c); Selectivity of the aptasensor to TB. Blank (a), 1 nmol·L<sup>-1</sup> PSA (b), 1 nmol·L<sup>-1</sup> HlgG (c), 1 nmol·L<sup>-1</sup> glucose (d), 0.1 nmol·L<sup>-1</sup> TB (e), 0.1 nmol·L<sup>-1</sup> TB + 1 nmol·L<sup>-1</sup> PSA (f), 0.1 nmol·L<sup>-1</sup> TB + 1 nmol·L<sup>-1</sup> HlgG (g), 0.1 nmol·L<sup>-1</sup> TB + 1 nmol·L<sup>-1</sup> glucose (h) (d). Error bars = RSD ( $n = 5$ )



### Optimization of experimental conditions

In order to obtain the optimal condition, the experimental conditions mostly containing the pH, the concentration of K<sub>2</sub>S<sub>2</sub>O<sub>8</sub> and Gr-Pt and the incubation time of TB solution were researched systematically. The results are shown in Fig. S5.

### Analytical performance of the ECL assay in TB detection

The modified working electrode was incubated with different concentrations of TB standard solutions and then detected in the 10 mL of PB (pH 7.5) containing 50 mmol·L<sup>-1</sup> K<sub>2</sub>S<sub>2</sub>O<sub>8</sub>. The continuous potential scanning was applied on the modified electrode from -1.8 V to 0 V at a scanning rate of 0.1 V·s<sup>-1</sup> and the PMT was set at 800 V. As shown in Fig. 4a, the ECL intensity decreases with the increasing TB concentrations in the range from 0 to 5.0 nmol·L<sup>-1</sup>. Fig. 4b shows the

equation of the calibration plot:  $\Delta I_{ECL} = 966.30 \log [c/\text{nmol}\cdot\text{L}^{-1}] + 6460.53$  ( $R = 0.994$ ).  $\Delta I_{ECL}$  is the change of ECL intensity ( $\Delta I_{ECL} = I_0 - I$ ,  $I_0$  and  $I$  being the ECL intensity of the modified working electrode before and after incubating with TB). The linear range is from  $1.0 \times 10^{-6}$  to 5.0 nmol·L<sup>-1</sup> with a detection limit of 0.35 fmol·L<sup>-1</sup> ( $S/N = 3$ ).

The results are compared with other methods as shown in Table 1. However, they used enzymes and metal-containing QDs in the comparative references. The denaturation and purification process of enzymes may be limit practical applications. And the metal-containing QDs are generally limited due to their toxicity, poor biocompatibility and stability. The PDANS@Ag/C-dots exhibits excellent ECL performance. The designed ECL assay shows a wider linear range and a lower detection limit for TB detection compared with other methods listed in Table 1.

### Stability, repeatability and selectivity of the ECL assay

The stability of the modified working electrode is a significant factor for the precise detection of TB. The stability investigation was carried out by continuous CV scanning for 13 cycles between -1.8 V and 0 V in PB (pH 7.5) containing 50 mmol·L<sup>-1</sup> K<sub>2</sub>S<sub>2</sub>O<sub>8</sub> using 0.1 nmol·L<sup>-1</sup> TB as a model. As depicted in

**Table 1** Comparison of our method with other methods for the determination of TB

Material	Detection method	Linear range (nmol·L <sup>-1</sup> )	Detection limit (nmol·L <sup>-1</sup> )	Ref.
G-quadruplex/hemin/HRP/AuPd	Voltammetric	$1.0 \times 10^{-4}$ - 20.0	$2.0 \times 10^{-5}$	[2]
Silver-coated glass/glucose oxidase	Fluorescence	0.3-6.5	0.082	[3]
CdTe QDs	Fluorescence	$5.0 \times 10^{-5}$ - 10.0	$1.5 \times 10^{-5}$	[4]
PANI-MWCNTs	Amperometric	$1.0 \times 10^{-4}$ - 4.0	$8.0 \times 10^{-5}$	[31]
CS@Fe <sub>3</sub> O <sub>4</sub> @GO@T-Apt@HM	Chemiluminescence	$5.0 \times 10^{-6}$ - 0.25	$1.5 \times 10^{-6}$	[32]
PDANS@Ag/C-dots	Electrochemiluminescence	$1.0 \times 10^{-6}$ - 5.0	$3.5 \times 10^{-7}$	This work

Fig. 4b, the ECL intensity shows no significant changes with the relative standard deviation (RSD) of 2.37%, which indicates the excellent stability for this assay. Six working electrodes prepared under same conditions were measured to test the repeatability. As shown in Fig. 4c, 1.74% of the RSD suggests the precision of the modified working electrode is considerable. In order to evaluate the selectivity, some biomolecules including prostate specific antigen (PSA), human IgG (HIgG), glucose were selected as the interfering substances. Fig. 4d shows that PSA, HIgG, and glucose exhibit no great decrease of the signal. In contrast to the incubation of the modified working electrode with  $0.1 \text{ nmol}\cdot\text{L}^{-1}$  TB, the large ECL intensity decrease is observed. The  $0.1 \text{ nmol}\cdot\text{L}^{-1}$  of TB containing  $1 \text{ nmol}\cdot\text{L}^{-1}$  of interfering substance was tested under the same experimental conditions. No obvious interferential signal is generated from the mixed sample, which indicates that the modified working electrode possessed good selectivity for the detection of TB.

## Conclusions

In summary, an ECL assay for TB detection is fabricated based on Gr-Pt as sensing platform and PDANS@Ag/C-dots as signal probe. The Gr-Pt nanocomposite is used to connect cDNA. Significantly, the ECL signal of C-dots is improved by anchoring on the PDANS@Ag due to effective immobilization of C-dots and Ag participation. The ECL assay has the capacity to determine TB from  $1.0 \times 10^{-6}$  to  $5.0 \text{ nmol}\cdot\text{L}^{-1}$  with a detection limit of  $0.35 \text{ fmol}\cdot\text{L}^{-1}$ . In addition, the ECL assay exhibits high sensitivity, good reproducibility, excellent stability and acceptable selectivity, suggesting a promising application in clinical diagnosis.

**Acknowledgements** This study was financially supported by the National Natural Science Foundation of China (21675063), the Science and Technology Planning Project of Higher Education of Shandong Province (J16LC23) and Q. Wei thanks the Special Foundation for Taishan Scholar Professorship of Shandong Province (No. ts20130937) and UJN.

**Compliance with ethical standards** The author(s) declare that they have no competing interests.

## References

- Wang Y, Luo W, Reiser G (2008) Trypsin and trypsin-like proteases in the brain: proteolysis and cellular functions. *Cell Mol Life Sci* 65(2):237–252
- Wang X, Sun D, Tong Y, Zhong Y, Chen Z (2017) A voltammetric aptamer-based thrombin biosensor exploiting signal amplification via synergetic catalysis by DNAzyme and enzyme decorated AuPd nanoparticles on a poly(o-phenylenediamine) support. *Microchim Acta* 184(6):1791–1799
- Li Y, Ling L (2015) Aptamer-based fluorescent solid-phase thrombin assay using a silver-coated glass substrate and signal amplification by glucose oxidase. *Microchim Acta* 182(9–10):1849–1854
- Wang GL, XL H, XM W, Dong YM, Li ZJ (2016) Fluorescent aptamer-based assay for thrombin with large signal amplification using peroxidase mimetics. *Microchim Acta* 183(2):765–771
- Liu J, Cao Z, Yi L (2009) Functional nucleic acid sensors. *Chem Rev* 109(5):1948
- Huang Y, Lei J, Cheng Y, Ju H (2015) Ratiometric electrochemiluminescence strategy regulated by electrocatalysis of palladium nanocluster for immunosensing. *Biosens Bioelectron* 77:733–739
- Fang L, Lü Z, Wei H, Wang E (2008) A electrochemiluminescence aptasensor for detection of thrombin incorporating the capture aptamer labeled with gold nanoparticles immobilized onto the thio-silanized ITO electrode. *Anal Chim Acta* 628(1):80–86
- Yuan Y, Han S, Hu L, Parveen S, Xu G (2012) Coreactants of tris(2, 2'-bipyridyl)ruthenium(II) electrogenerated chemiluminescence. *Electrochimica Acta* 82 (complete):484–492
- Xu Y, Yin XB, He XW, Zhang YK (2015) Electrochemistry and electrochemiluminescence from a redox-active metal-organic framework. *Biosens Bioelectron* 68(1):197–203
- Li J, Guo S, Wang E (2012) ChemInform abstract: recent advances in new luminescent nanomaterials for electrochemiluminescence sensors. *RSC Adv* 43(2):3579–3586
- Michalet X, Pinaud FF, Bentolila LA, Tsay JM, Doose S, Li JJ, Sundaresan G, Wu AM, Gambhir SS, Weiss S (2005) Quantum dots for live cells, in vivo imaging, and diagnostics. *Science* 307(5709):538–544
- Krysmann MJ, Kellarakis A, Dallas P, Giannelis EP (2012) Formation mechanism of carbogenic nanoparticles with dual photoluminescence emission. *Journal of the American Chemical Society* 134 (2):747–750
- Wang J, Zhao WW, Li XR, JJ X, Chen HY (2012) Potassium-doped graphene enhanced electrochemiluminescence of  $\text{SiO}_2$ @CdS nanocomposites for sensitive detection of TATA-binding protein. *Chem Commun* 48(51):6429–6431
- Li NL, Jia LP, Ma RN, Jia WL, Lu YY, Shi SS, Wang HS (2016) A novel sandwiched electrochemiluminescence immunosensor for the detection of carcinoembryonic antigen based on carbon quantum dots and signal amplification. *Biosens Bioelectron* 89:453–460
- Fang L, Deng W, Yan Z, Ge S, Yu J, Song X (2014) Application of ZnO quantum dots dotted carbon nanotube for sensitive electrochemiluminescence immunoassay based on simply electrochemical reduced Pt/au alloy and a disposable device. *Anal Chim Acta* 818:46–53
- Zhou H, Ning G, Li T, Cao Y, Zeng S, Lei Z, Guo Z (2012) The sandwich-type electrochemiluminescence immunosensor for  $\alpha$ -fetoprotein based on enrichment by  $\text{Fe}_3\text{O}_4$ -au magnetic nano probes and signal amplification by CdS-au composite nanoparticles labeled anti-AFP. *Anal Chim Acta* 746:107
- Qiang W, Li W, Li X, Chen X, Xu D (2014) Bioinspired polydopamine nanospheres: a superquencher for fluorescence sensing of biomolecules. *Chem Sci* 5(8):3018–3024
- Lee H, Dellatore SM, Miller WM, Messersmith PB (2007) Mussel-inspired surface chemistry for multifunctional coatings. *Science* 318(5849):426–430
- Cui J, Yan Y, Such GK, Liang K, Ochs CJ, Postma A, Caruso F (2012) Immobilization and intracellular delivery of an anticancer drug using mussel-inspired polydopamine capsules. *Biomacromolecules* 13(8):2225
- Ye Q, Zhou F, Liu W (2011) ChemInform abstract: bioinspired catecholic chemistry for surface modification. *Chem Soc Rev* 40(7):4244



21. Dreyer DR, Miller DJ, Freeman BD, Paul DR, Bielawski CW (2013) Perspectives on poly(dopamine). *Chem Sci* 4(10):3798–3802
22. Liu Y, Zhao Y, Zhu Z, Xing Z, Ma H, Wei Q (2017) Ultrasensitive immunosensor for prostate specific antigen using biomimetic polydopamine nanospheres as an electrochemiluminescence superquencher and antibody carriers. *Anal Chim Acta* 963:17–23
23. Li L, Nurunnabi N, Lee YK, Huh KM (2013) GSH-mediated photoactivity of pheophorbide a-conjugated heparin/gold nanoparticle for photodynamic therapy. *J Control Release Soc* 171(2):241
24. Deng S, Ju H (2013) Electrogenerated chemiluminescence of nanomaterials for bioanalysis. *Analyst* 138(1):43–61
25. Marcano DC, Kosynkin DV, Berlin JM, Sinitskii A, Sun Z, Slesarev A, Alemany LB, Lu W, Tour JM (2010) Improved synthesis of graphene oxide. *ACS Nano* 4(8):4806–4814
26. Dong Y, Shao J, Chen C, Li H, Wang R, Chi Y, Lin X, Chen G (2012) Blue luminescent graphene quantum dots and graphene oxide prepared by tuning the carbonization degree of citric acid. *Carbon* 50(12):4738–4743
27. Yan J, Yang L, Lin MF, Ma J, Lu X, Lee PS (2013) Polydopamine spheres as active templates for convenient synthesis of various nanostructures. *Small* 9(4):596–603
28. Nan Z, Weiguang M, Dongxue H, Lingnan W, Tongshun W, Li N (2015) The fluorescence detection of glutathione by •OH radicals' elimination with catalyst of MoS<sub>2</sub>/rGO under full spectrum visible light irradiation. *Talanta* 144:551–558
29. Teng X, Yang H (2009) Synthesis of face-centered tetragonal FePt nanoparticles and granular films from Pt@Fe<sub>2</sub>O<sub>3</sub> core-shell nanoparticles. *Journal of the American Chemical Society* 125 (47): 14559–14563
30. Sun Y, Ren Q, Liu B, Qin Y, Zhao S (2016) Enzyme-free and sensitive electrochemical determination of the FLT3 gene based on a dual signal amplified strategy: controlled nanomaterial multilayers and a target-catalyzed hairpin assembly. *Biosens Bioelectron* 78:7–13
31. Su Z, Xu X, Xu H, Zhang Y, Li C, Ma Y, Song D, Xie Q (2017) Amperometric thrombin aptasensor using a glassy carbon electrode modified with polyaniline and multiwalled carbon nanotubes tethered with a thiolated aptamer. *Microchim Acta* 184(6):1677–1682
32. Sun Y, Wang Y, Li J, Ding C, Lin Y, Sun W, Luo C (2017) An ultrasensitive chemiluminescence aptasensor for thrombin detection based on iron porphyrin catalyzing luminescence desorbed from chitosan modified magnetic oxide graphene composite. *Talanta* 174:809